Hydrological Processes
*Hydrol. Process.* **12**, 1569–1587 (1998)

# The sensitivity of snowmelt processes to climate conditions and forest cover during rain-on-snow: a case study of the 1996 Pacific Northwest flood

Danny Marks,[1]* John Kimball,[2] Dave Tingey[3] and Tim Link[4]

[1]*USDA-ARS, Northwest Watershed Research Center, 800 Park Blvd., Suite 105, Boise, ID 83712, USA*
[2]*University of Montana, NTSG School of Forestry, Missoula, MT 59812, USA*
[3]*EPA National Health and Environmental Effects Research Lab., Corvallis, OR 97333, USA*
[4]*Oregon State University, College of Oceanic and Atmosheric Sciences, Corvallis, OR 97333, USA*

## Abstract:

A warm, very wet Pacific storm caused significant flooding in the Pacific Northwest during February 1996. Rapid melting of the mountain snow cover contributed to this flooding. An energy balance snowmelt model is used to simulate snowmelt processes during this event in the Central Cascade Mountains of Oregon. Data from paired open and forested experimental sites at locations at and just below the Pacific Crest were used to drive the model. The event was preceded by cold, stormy conditions that developed a significant snow cover down to elevations as low as 500 m in the Oregon Cascades. At the start of the storm, the depth of the snow cover at the high site (1142 m) was 1·97 m with a snow water equivalent (SWE) of 425 mm, while at the mid-site (968 m) the snow cover was 1·14 m with a SWE of 264 mm. During the 5–6 day period of the storm the open high site received 349 mm of rain, lost 291 mm of SWE and generated 640 mm of runoff, leaving only 0·22 m of snow on the ground. The mid-site received 410 mm of rain, lost 264 mm of SWE to melt and generated 674 mm of runoff, completely depleting the snow cover. Simulations at adjacent forested sites showed significantly less snowmelt during the event. The snow cover under the mature forest at the high site lost only 44 mm of SWE during the event, generating 396 mm of runoff and leaving 0·69 m of snow. The model accurately simulated both snow cover depth and SWE during the development of the snow cover prior to the storm, and the depletion of the snow cover during the event. This analysis shows that because of the high temperature, humidity and relatively high winds in the open sites during the storm, 60–90% of the energy for snowmelt came from sensible and latent heat exchanges. Because the antecedent conditions extended the snow cover to very low elevations in the basin, snowmelt generated by condensation during the event made a significant contribution to the flood. Lower wind speeds beneath the forest canopy during the storm reduced the magnitude of the turbulent exchanges at the snow surface, so the contribution of snowmelt to the runoff from forested areas was significantly less. This experiment shows the sensitivity of snowmelt processes to both climate and land cover, and illustrates how the forest canopy is coupled to the hydrological cycle in mountainous areas. © 1998 John Wiley & Sons, Ltd.

KEY WORDS snowmelt; rain-on-snow; forest canopy effects; flooding

## INTRODUCTION AND BACKGROUND

Rain-on-snow events are a common occurrence on mountain slopes within the snow transition zone of the Pacific Northwest. This zone extends from approximately 300–1000 m in elevation throughout the western

* Correspondence to: Dr D. Marks, USDA-ARS, Northwest Watershed Research Center, 800 Park Blvd., Suite 105, Boise, ID 83712, USA.

Contract grant sponsor: US Environmental Protection Agency.
Contract grant number: DW 14936911.

CCC 0885–6087/98/111569–19$17·50


*Received 25 May 1997*
*Accepted 27 March 1998*

Oregon and Washington, coastal British Columbia and California (Beaudry and Golding, 1983; Harr, 1986). The region is characterized by a maritime climate with moderate winter temperatures. Rainfall, mixed rain and snow, or snowfall occurs frequently during the winter months from the moist frontal systems that move in from the Pacific ocean. Annual precipitation (rain and snow) frequently exceeds 2000 mm, and the seasonal snow cover can exceed depths of 5–7 m at elevations above 2500 m. Extension of the seasonal snow cover down into the snow transition zone is dependent on climate conditions during the winter. In this zone, however, snowpacks are generally shallow with temperatures at or near 0·0 °C. Under these conditions little energy is needed to initiate melt. The snow cover within this region is dynamic and can experience successive periods of accumulation and ablation during the winter months. It is not uncommon for an entire snowpack to melt during a single rainfall event. During warm or rainy periods the snowpack yields runoff quickly owing to a low capacity for storage of liquid water once melting conditions are achieved (Colbeck, 1978; Berris and Harr, 1987).

Harvesting of forests in the snow transition zone is a common occurrence throughout the Pacific Northwest. In cleared or exposed areas, such as those resulting from clear-cut logging practices, advective energy from rainfall, combined with increased turbulence, is suspected of enhancing snowmelt (Beaudry and Golding, 1983; Harr, 1986; Berris and Harr, 1987; Coffin and Harr, 1992; van Heeswijk *et al*., 1996), and increasing erosion and downstream flooding during rainfall events (Waananen *et al*., 1971; Jones and Grant, 1996). Unfortunately, detailed data on climate conditions, snow properties and snowmelt processes during rain-on-snow conditions are very limited. The few detailed snow and climate monitoring programmes that have been conducted in alpine or mountainous regions have been done at elevations well above the snow transition zone, or restricted to forest clearings or unforested sites (e.g. Anderson, 1976; Smith and Berg, 1982; Davis *et al*., 1984; Marks *et al*., 1986, 1992).

None of these efforts were specifically established to monitor rain-on-snow events, and none were designed to evaluate the differences between forested and unforested sites. Several studies of rain-on-snow processes have been conducted, but the data from these have been limited to air temperature, with some event precipitation and snow properties measurements below the canopy. Berris and Harr (1987) investigated the effect that clear-cutting has on snow processes during rain-on-snow in the Oregon Cascades. They monitored snow deposition and melt in adjacent forested and clear-cut sites in the H.J. Andrews Experimental Forest during the 1983 and 1984 water years. Some meteorological parameters and lysimeter data were collected in both plots during part of that time period. While some problems occurred with both the methods used and the instruments selected, as reported by the authors, this was by far the best data set characterizing snow processes and properties during rain-on-snow in forested and clear-cut plots. Unfortunately, the snow cover was thin and discontinuous during most of the study, and only a few, relatively small rain-on-snow events occurred. Berris and Harr (1987) were able to show that significantly more snowmelt was generated in the clear-cut, and that much of this difference was due to enhanced sensible and latent heat flux caused by higher wind. However, the largest absolute difference was only 11 mm over the period of a 3-day event in February 1984, which is within the noise or uncertainty expected from eight small (0·25 $m^2$) meltwater collection pans, particularly those located beneath a forest canopy (Kattelmann, 1989). Although the conclusions of Berris and Harr (1987) were correct based on the physics and processes involved, the limitations of the data and conditions during their experiment rendered the study somewhat inconclusive.

van Heeswijk *et al*. (1996), using the Barris and Harr data set, did additional analysis to show the sensitivity of snowmelt to increases in wind, air temperature and the magnitude of precipitation during a rain-on-snow event. Using a modified version of an energy balance snowmelt model originally developed by Marks (1988), they did multiple simulations of the snow cover energy and mass balance during several events that occurred in February 1984, to investigate the departure from the base snowmelt conditions reported by Berris and Harr (1987) when air temperature (which was assumed to be dew point temperature during the event), precipitation and wind were increased. Their results indicated that while higher rainfall rates have little effect on the production of snowmelt, and higher temperatures have only a modest effect, higher wind speeds can significantly increase snowmelt. Doubling precipitation added only 0·1–0·5 mm snowmelt for the three events, while

 

adding 2 °C to the air temperature increased snowmelt by 0·7–5·8 mm. Wind speeds during the events were low, averaging 1·7 to 2·1 $ms^{-1}$. Increasing these by four times produced an additional 6·1–61 mm of snowmelt, and increasing them by six times produced an additional 10–100 mm snowmelt. If both temperature (+2 °C), and wind (4×) are increased at the same time, as much as 135 mm of additional snowmelt could be generated.

From this analysis we can conclude that the generation of snowmelt during rain-on-snow is most sensitive to wind speed, but also sensitive to high temperature and humidity if they occur in conjunction with high winds. Advection from rain falling on snow does not enhance snowmelt generation. In the snow transition zone, higher wind speeds generally occur in clearings or clear-cuts. However, as Berris and Harr (1987) illustrate, these conditions do not occur frequently. If a rain-on-snow event with very high winds, temperatures, humidity and precipitation were to occur at a time when a significant snow cover was in place across much of the snow transition zone, it has the potential to produce significant snowmelt which would enhance runoff, and increase the potential for flooding.

In this paper, we analyse snow properties, processes and melt during such an event. Using data from experimental monitoring sites located in clear-cuts, and under adjacent mature forests, we present the differences in air and soil temperature, humidity, wind, radiation, precipitation and snow depth conditions in open and forested locations, both prior to, and during one of the most significant rain-on-snow events on record for the Oregon Cascades. We use these data to drive a snow cover energy balance model to simulate development of the snow cover prior to the event, and then ablation of that snow cover during and after the event. The results of this simulation are compared with continuously monitored snow depths at the experimental sites, and to changes in snow water equivalent (SWE) measured at nearby National Resources Conservation Service (NRCS) SNOTEL stations.

## EXPERIMENTAL SITES

During 1993, several intensive field sites were established in a transect from the foothills just above the Willamette Valley, to the crest of the Central Oregon Cascades by EPA scientists working at the National Health and Environmental Effects Research Laboratory (NHEERL) in Corvallis, Oregon. The sites are located along the Oregon Highway 20 corridor leading from Sweet Home, Oregon, to the Santiam Junction. In 1994 meteorological monitoring was initiated in open forest clear-cuts at these sites, and in 1995 meteorological monitoring was extended to nearby mature forest locations near the open monitoring stations at two of the sites. The purpose of these field sites is to provide data to characterize how ecological processes and the composition of forests in the Western Cascade mountains of Oregon and Washington vary in response to climatic gradients and variability, soil type, management activities, successional stage and disturbances such as fire, insects, floods and landslides.

Figure 1 shows both the elevational gradient and the location of the Cascade experimental sites on a shaded relief map of north-western Oregon. With a reference site at the EPA NHEERL in Corvallis, OR, (80 m), field sites are located at 536 m, [just above Cascadia, OR (the low site)], at 929 m [just below Tombstone Pass (the mid-site)] and at 1142 m [between Tombstone Pass and Santiam Junction (the high site)].

At the low and high sites, meteorological monitoring systems were establish both in a forest clear-cut and in an adjacent mature forest. Meteorological monitoring was established only in a clear-cut at the mid-site. At each of these sites a suite of meteorological, atmospheric, snow and soil parameters are monitored continuously throughout the year. Only data from the high and mid-sites were used for this analysis, because there was little snow accumulation at the low site. Table I lists all of the parameters monitored at the high and mid sites.

Much of the annual precipitation in the Oregon Cascades falls as snow at elevations above 500 m. While snow can occur down to the valley floor (near sea level), it is infrequent at elevations below 350 m, and a persistent continuous snow cover is rarely established at elevations below 600 m. The low site is below this

 

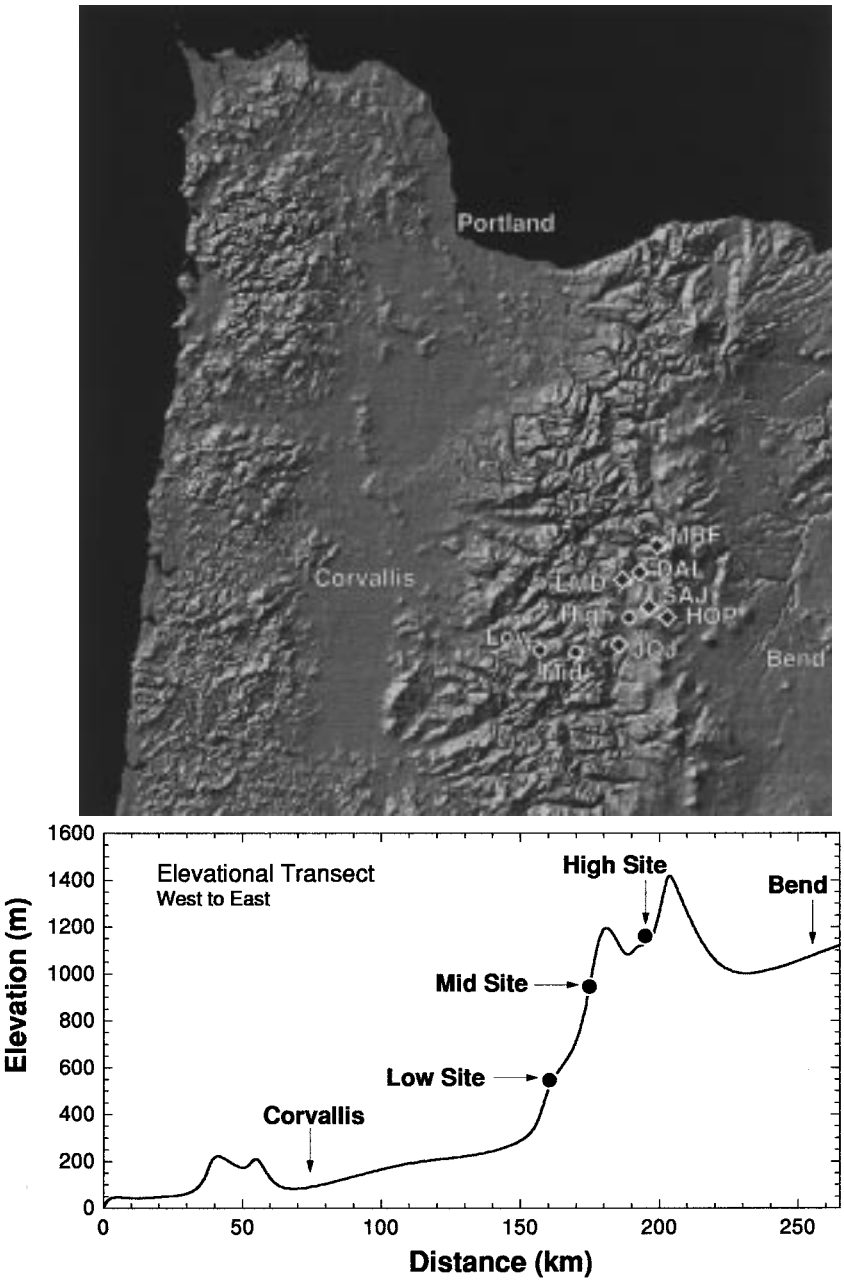


Figure 1. The elevational gradient and location of the three experimental sites on a shaded relief map of north-western Oregon. NRCS SNOTEL stations used in this analysis are also located on the shaded relief map, indicated by the three-letter designations shown in Figure 2

elevation, and is not really in the snow transition zone. Therefore, snow monitoring was done only at the mid- and high sites and only data from these sites is used in this analysis. Both the mid- and high sites are located in the snow transition zone where significant rain, mixed rain and snow or cold snow deposition may occur during the winter season (Beaudry and Golding, 1983; Harr, 1986).

 

Table I. Meteorological data collected at EPA field sites (most data collected as hourly averages

| Parameters | Mid-site (929 m) | High site (1142 m) | |
|---|---|---|---|
| | Clear-cut | Clear-cut | Forest |
| Air temperature (°C) | * | * | * |
| Relative humidity (%) | * | * | * |
| Solar radiation (PAR) (400–700 nm) | * | * | * |
| Solar radiation (Total: 280–2800, NIR: 700–2800 nm) | * | | |
| Precipitation* (mm $h^{-1}$) | * | * | * |
| Wind speed (m $s^{-1}$) | * | * | * |
| Soil temp. (15, 30 cm) | * | * | * |
| Soil moisture (TDR) | * | * | * |
| Snow depth (m) | * | * | |

* At the EPA field sites, precipitation was monitored using unshielded and unheated tipping bucket gauges. Data from these gauges provide a reasonable estimate of rainfall, but not a reliable measure of snowfall. Snowfall depths were, however, monitored using sonic depth sensors.

## THE FEBRUARY 1996 FLOOD

The 1996 water year (October 1995 to September 1996) was one of the wettest on record, and included a number of extreme climatic events that combined to set the stage for a major flood event during February 1996. The autumn and early winter period (October 1995 to mid-January 1996) was unusually wet, but warm, with very little snowfall below 1500 m. Low elevation NRCS SNOTEL measurement stations in the central Oregon Cascade Mountains recorded no snow, and higher elevation stations reported a snow water equivalent (SWE) of approximately 25% of the long-term average for early January. In mid-January a series of colder storms deposited significant amounts of snow down to 600 m, which is well below the elevation of the lowest SNOTEL station in Oregon (800 m, Marion Forks, in the Santiam Basin). By the third week in January, most of the SNOTEL stations in the central Cascades reported SWE of between 100 and 140% of the long-term average for that data.

The last week in January was one of the coldest on record for the central and northern Cascades. Temperatures were well below freezing from 27 January to 2 February, with high winds, low humidities and many stations reporting low temperatures in the −10 to −20 °C range. On 2 February temperatures began to warm. A moderate storm deposited rain and freezing rain on already frozen soils and on the very cold snowpack.

Then on 3 February 1996, a warm, very humid storm system from the Southern Pacific hit the coast of Oregon. This event lasted nearly six days in the northern and central Cascades. The 3–8 February event was accompanied by high winds and intense rainfall, and was one of the most intense rain-on-snow (ROS) events ever recorded. It deposited record amounts of rain across the northern and central Cascade Mountains of Oregon. Many stations approached or exceeded historical event rainfall records, most of which were established during the December 1964 flood. Stations in the northern and central Cascades reported rainfall of 300 to 500 mm during the first phase of the event.

During this ROS event, SNOTEL stations on the western side of the Cascade crest reported SWE losses of 35 to 100%. Intense rainfall combined with rapid snowmelt contributed to a flood event that was comparable in magnitude to the December 1964 flood, which was the largest recorded in the Northwest. Peak flows on headwater streams and rivers draining the northern and central Cascades occurred around 8 February.

During the warm sunny period that followed 9–15 February, humidities were low, with dew point temperatures generally below freezing, and wind speeds were significantly less. Snowmelt continued at a much more moderate rate at those sites that still had snow. By 16 February, flood waves in the headwater

 

Table II. Precipitation, snowmelt and water available for runoff (WAR) for SNOTEL stations nearest central Cascade experimental sites during the six day ROS event (3–8 February 1996)

| SNOTEL station | Elevation (m) | Precipitation (mm) | SWE loss (mm) | WAR (mm) | Snowmelt % WAR |
|---|---|---|---|---|---|
| Little Meadows | 1220 | 361 | 330 | 691 | 48 |
| Marion Forks | 800 | 300 | 389 | 689 | 57 |
| Daly Lake | 1100 | 279 | 211 | 490 | 48 |
| Hogg Pass | 1450 | 277 | 137 | 414 | 33 |
| Jump-Off-Joe | 1070 | 320 | 84 | 404 | 21 |
| Santiam Jct. | 1145 | 229 | 79 | 308 | 26 |

streams of the northern and central Cascades had passed, and flows had returned to normal. By the end of this period, very little snow existed at elevations below 1000 m.

A second storm occurred from 16–22 February. It started as a rain event, with high humidities and temperatures above freezing. However, wind speeds were significantly lower than during the 3–8 February period, with temperatures and humidities steadily dropping. By 20 February, precipitation had turned to snow, and most SNOTEL stations were reporting increasing SWE.

Table II shows reported precipitation (rain and snow), loss of SWE, estimated water available for runoff (WAR, the combination of rain plus snowmelt) and the relative contribution of snowmelt to WAR for SNOTEL stations (USDA Soil Conservation Service, 1988) nearest the Central Cascade Experimental sites during the six days 3–8 February) of the ROS event. Air temperature and changes in SWE were used to determine whether precipitation was rain or snowfall at higher elevation stations. Some snowfall probably occurred during the early part of the event at Hogg Pass. Precipitation volumes are remarkably consistent at all stations except Little Meadows. It is possible that some of the reported precipitation at that site is the result of a plug of snow that was lodged in the gauge during the January snow event being added to the total during the ROS event. However, the raw SNOTEL data show steady precipitation during the event.

The first three SNOTEL stations listed in Table II reported more SWE loss, and therefore more WAR than the last three. The higher elevation station (Hogg Pass) is at the upper end of the snow transition zone. It had cooler temperatures, some snowfall and generated less snowmelt during the event than Little Meadows, Marion Forks or Daly Lake. Santiam Jct. is just east of the crest of the western Cascades where temperatures during the event were cooler, and wind speeds were less. Jump-Off-Joe is a protected and shaded site that seems to respond differently than the other sites in or near the South Santiam Basin.

Figure 2 shows hourly traces from six of the nearest SNOTEL stations, daily rainfall recorded at the mid- and high experimental sites and half-hourly stream discharge from the South Santiam River just above Foster Lake from 1 January to 1 March 1996. Although there were several rainfall events in early January, the response of the South Santiam River was damped, rising from 40 $m^3 s^{-1}$ to 80 or 100 $m^3 s^{-1}$. During the February ROS event, the river rose from just below 20 $m^3 s^{-1}$ on 3 February to nearly 900 $m^3 s^{-1}$ by 8 February.

The Marion Forks, Daly Lake and Little Meadows SNOTEL stations all show a rapid loss of SWE in response to the storm. Hogg Pass is clearly above the snow transition zone, losing some SWE in response to the storm, but actually ending up with a net gain in SWE by the end of February. Jump-Off-Joe and Santiam Jct. show only a small decrease in SWE, and by the end of February are essentially back to where they started. Although these two stations are within the snow transition zone, it is clear from the data that they are located at sites that were climatically different during the ROS event from conditions that occurred at Marion Forks, Daly Lake and Little Meadows. Throughout the event the SWE loss at these three SNOTEL stations is about the same magnitude as rainfall. During the period 3–8 February 1996, SNOTEL data indicate that 490 mm of water available for runoff (WAR) was generated at Daly Lake, over 689 mm of WAR at Marion

 

Forks and over 691 mm of WAR at Little Meadows. Of the water available for runoff, SWE loss contributed between 48 and 57%.

This was a significant snowmelt flood that occurred during ideal rain-on-snow conditions. It provides us with the opportunity to investigate how the combination of climate conditions prior to the event, combined with the conditions that occurred during the event, led to rapid depletion of the snow cover. It also provides an opportunity to evaluate how the presence or absence of forest cover in the snow transition zone may affect these processes. To perform this analysis, we use an energy balance snowmelt model, with detailed data collection at three experimental sites within the snow transition zone to simulate the thermodynamic processes occurring during the event, both in a forest clear-cut and beneath a mature forest.

## A TWO-LAYER, ENERGY BALANCE SNOWMELT MODEL

In a seasonal snow cover, snow is thermodynamically unstable, undergoing continuous metamorphism until it melts and becomes runoff during spring (Colbeck, 1982). These metamorphic changes and final melting are driven by temperature and vapour density gradients within the snow cover, which are caused by heat exchange at the snow surface and at the snow–soil interface (Colbeck *et al.*, 1979; Male and Granger, 1981). In general, the energy balance of a snow cover is expressed as

$$\Delta Q = R_n + H + L_v E + G + M \tag{1}$$

where $\Delta Q$ is change in snow cover energy, and $R_n$, $H$, $L_v E$, $G$ and $M$ are net radiative, sensible, latent, conductive and advective energy fluxes (all terms are in $\mathrm{Wm}^{-2}$). In thermal equilibrium, $\Delta Q = 0$; a negative energy balance will cool the snow cover, increasing its cold content (the amount of energy in $\mathrm{Jm}^{-2}$ required to bring it to 0·0 °C), while a positive energy balance will warm the snow cover. The snow cover cannot be warmer than 0·0 °C, and melt cannot occur in significant amounts until the entire snow cover has reached this temperature. Once the entire snow cover is isothermal at 0·0 °C, positive values of $\Delta Q$ must result in melt.

Below we present a brief description of the model (see Energy and mass balance calculations) that was used to simulate the development of the snow cover at the experimental sites prior to the February 1996 rain-on-snow event, and then the ablation of that snow cover during and after the event. The model simulates each component of the snow cover energy balance, accumulates mass and either develops a snow cover or calculates melt and runoff, and then adjusts snow cover mass and thermal conditions for the next time-step.

The snowmelt model is initialized by measurement heights and snow cover state variables (snow depth, density, temperature and liquid water content) if the snow cover exists at the start of the run.[1] It is then driven by independent inputs of net solar radiation and meteorological parameters, including precipitation mass, temperature and estimated density, to calculate the energy and mass balance and runoff from the snow cover. It predicts melt in two snow cover layers, runoff from the base of the snow cover and adjusts the snow cover mass, thickness, thermal properties and measurement heights at each time-step. The modelling approach is an adaptation of the model developed by Marks (1988), and Marks and Dozier (1992). The modelling approach is similar to that used by Anderson (1976), Morris (1982, 1986), Jordan (1991) and Tarboton *et al.* (1995), but the data requirements are simpler and more generalizable. Table III presents the state variables and forcing variables required by the model. State variables are input as initial conditions, and then predicted by the model during the run. Forcing variables are used by the model to predict the state variables, and are input at each time-step of the model run.

A complete description of the model, its input requirements and output parameters can be found in Marks *et al.* (1998). Figure 3 is a schematic diagram of the model structure and components.

[1] For this analysis no snow was present at the start of the simulation, so initial conditions were set to zero, and the snow cover depth, density and properties were generated by the model from meteorological conditions during the simulation period.

 

Table III. State variables predicted by the model and forcing variables required by the model

| State variables | Forcing variables |
|---|---|
| Snow depth (m) | Net solar radiation ($Wm^{-2}$) |
| Snow density (kg $m^{-3}$) | Incoming thermal radiation ($Wm^{-2}$) |
| Snow surface layer temperature (°C) | Air temperature (°C) |
| Average snow cover temperature (°C) | Vapour pressure (Pa) |
| Average snow liquid water content (%) | Wind speed (m $s^{-1}$) |
| | Soil temperature (°C) |

*Energy and mass balance calculations*

A detailed discussion of energy and mass transfer over a snow surface was presented by Marks (1988), and is further discussed by Marks and Dozier (1992) and Marks *et al*. (1992). Presented below is a brief description of the equations solved, followed by a description of the structure of the model. Once the initial snow cover and measurement height parameters are set, the thermal, mass and wetness conditions of the snow cover are calculated. The thickness of the lower snow layer is set as the difference between the total

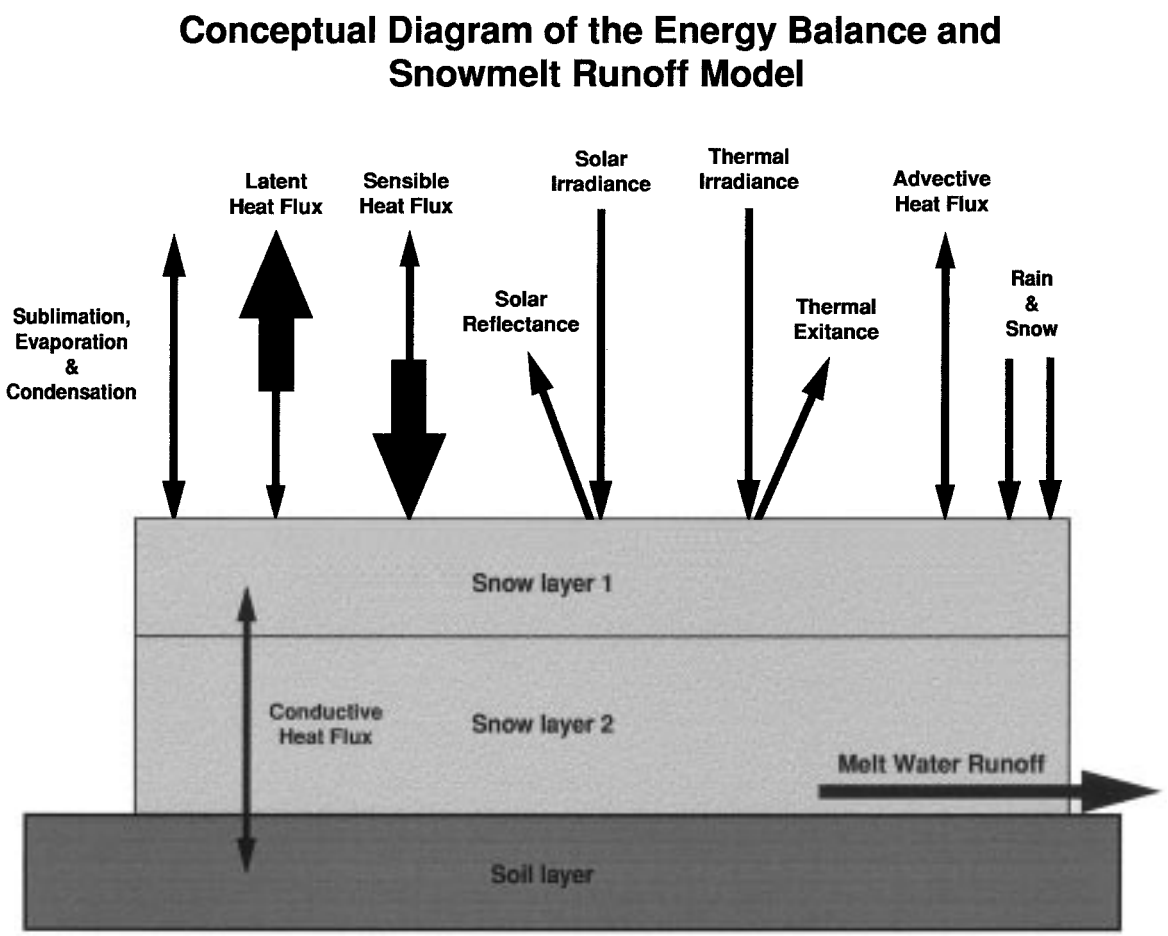


Figure 3. Schematic diagram of the snowmelt model structure and components

 

snow cover thickness, and the thickness of the surface active snow layer. The specific mass[2] of each layer, and the whole snow cover, is calculated from layer thickness and average snow cover density.

The temperature (K) of the snow surface layer and average temperature for the entire snow cover are either set from initial snow conditions or calculated at the end of the last model time-step. The temperature of the lower snow layer is set as a proportion of the snow cover mass in the lower layer. The cold contents are calculated from the specific heat of ice, the layer temperature and the specific mass. The specific heat of ice for each layer is calculated as a function of layer temperature.

The maximum liquid water holding capacity, $w_{c,max}$ of the snow cover is a volume ratio defined as follows (Davis *et al.*, 1985).

$$w_{c,max} = \frac{\text{Volume of water}}{\text{Volume of snow} - \text{Volume of ice}}$$

It is the capacity of the void fraction of the snow cover to hold liquid water and is used to determine the relative saturation of the snow cover in the calculation of runoff. $w_{c,max}$ is set as a constant (usually 0·01) at the beginning of the model run. The initial relative saturation of the snow cover is set as an initial condition. From these two parameters the liquid water content of the snow cover and the maximum liquid water content (kg $m^{-2}$) are derived, adjusted and updated during each time-step.

If a precipitation event occurs, the model adjusts mass, depth, liquid water content, temperature and density. A precipitation input includes time since the start of the run, total precipitation mass, percentage of the total mass that was snow, average density of the snow portion and average precipitation temperature. If snowfall or a mixed rain/snowfall event occurs, the temperature of the surface snow layer, the average temperature of the snow cover, the thickness of the lower snow layer and the thickness of the snow cover, the average density of the snow cover, the relative liquid water saturation and the liquid water content are adjusted. If the precipitation temperature is equal to, or greater than, the melting temperature of ice (0 °C) and the percentage snow is set to less than 1·0, then the model assumes that rain has occurred. For a mixed rain/snow event, the temperature of the snow portion is set to 0 °C and the liquid water content to saturation. The temperature of the rain portion is always set to either 0 °C or the input precipitation temperature, whichever is greater. If the precipitation temperature is equal to 0 °C and the percentage snow is 1·0 (a warm snow event), the temperature of the snow is set to 0 °C and the liquid water content is set to 1·0 (saturation). If the input precipitation temperature is less than 0 °C (a cold snow event), the temperature of the snow is set to the input precipitation temperature, and the liquid water content is set to 0.

If rain occurs, snow cover compaction is estimated from rainfall intensity over the time-step, and snow cover thickness, densities and relative liquid water saturation are adjusted. If a warm rain event occurs, without snow, only adjustments from compaction and addition of liquid water are made. If rain occurs in the absence of a snow cover, the volume of water added becomes runoff.

After the snow cover thermal conditions have been set, the model reads the input data to calculate the energy balance of the snow cover for that time-step. Net radiation, $R_n$ ($Wm^{-2}$), is calculated by

$$R_n = R_{n,sol} + I_{lw} - (\varepsilon_s \sigma \, {T_{s,0}}^4) \tag{2}$$

Net solar radiation, $R_{n,sol}$ ($Wm^{-2}$) and thermal irradiance, $I_{lw}$ ($Wm^{-2}$), are inputs; $\sigma$ is the Stefan–Boltzmann constant ($5{\cdot}6697 \times 10^{-8}$ J $m^{-2}$ $K^{-4}$); the temperature of the surface layer $T_{s,0}$ begins at the initial input value and is then calculated and updated at the end of each time-step by the model. Surface emissivity, $\varepsilon_s$, is set at a constant value of 0·99 by the model.

[2] Specific mass is defined as 'mass per unit area', or in this case: mass $m^{-2}$. For snow, it can be converted directly into a depth of water, in mm, because: a kg of water $m^{-2}$ = a mm of water $m^{-2}$.

 

Turbulent transfer terms, $H$ ($Wm^{-2}$) and $L_vE$ ($Wm^{-2}$), are calculated using a method adapted from Brutsaert (1982) by Marks and Dozier (1992) as a system of non-linear equations that simultaneously solve for the Obukhov stability length, $L$, the friction velocity, $u^*$, and the sensible heat flux, $H$, and the mass flux by evaporation or condensation from the snow surface, $E$ (kg $m^{-2}$ $s^{-1}$)

$$L = \frac{u^{*3}\rho}{kg\left[\frac{H}{T_a C_p} + 0{\cdot}61E\right]} \tag{3}$$

$$u^* = \frac{uk}{\ln\left[\frac{z_u - d_0}{z_0}\right] - \psi_{sm}\left[\frac{z_u}{L}\right]} \tag{4}$$

$$H = \frac{(T_a - T_{s,0})\, a_H\, k\, u^* \rho\, C_p}{\ln\left[\frac{z_r - d_0}{z_0}\right] - \psi_{sm}\left[\frac{z_T}{L}\right]} \tag{5}$$

$$E = \frac{(q - q_{s,0})\, a_E\, k\, u^* \rho}{\ln\left[\frac{z_q - d_0}{z_0}\right] - \psi_{sv}\left[\frac{z_q}{L}\right]} \tag{6}$$

$\rho$ is the density of the air, $k$ is the von Karman constant ( $\approx 0{\cdot}40$), $g$ is the acceleration due to gravity (9·80616 m $s^{-2}$), $C_p$ is the specific heat of dry air at constant pressure (1005J $kg^{-1}$ $K^{-1}$), $E$ is the mass flux by evaporation or condensation from the snow surface (kg $m^{-2}$ $s^{-1}$), $u$ is the wind speed (m $s^{-1}$), $d_0$ is the zero-plane displacement height (m, $\approx (2/3)7{\cdot}35\ z_0$), $a_H$ and $a_E$ are the ratio of eddy diffusivity and viscosity for heat and water vapour [Brutsaert (1982) suggests $a_H = a_E = 1{\cdot}0$)], and $\psi_{sm}$, $\psi_{sh}$, and $\psi_{sv}$ are stability functions for mass, heat and water vapour (positive when stable, negative when unstable, and 0 for neutral stability) [see Marks and Dozier (1992) for a detailed description of the stability functions]. The measurement heights for temperature, humidity and wind (m), $z_T$, $z_q$, and $z_u$ are set as initial conditions and then updated by the model as the depth of the snow cover changes. The roughness length, $z_0$ (m), is set as a constant at the beginning of the run, but can be updated as conditions require. Air temperature, $T_a$ (K), wind speed, $u$ (m $s^{-1}$) and vapour pressure, $e_a$ (Pa) are model inputs, and specific humidity, $q$ (g $kg^{-1}$), is calculated from $e_a$ and site air pressure. Snow surface layer temperature, $T_{s,0}$ (K), is adjusted by the model at the end of each time-step; snow surface specific humidity is calculated as a function of site air pressure and the saturation vapour pressure at $T_{s,0}$. The latent heat flux, $L_vE$ ($Wm^{-2}$), is $L_v \times E$, where $L_v$ is the latent heat of fusion (J $kg^{-1}$), which varies with the temperature and state of the water (liquid or solid) from $2{\cdot}501 \times 10^6$ J $kg^{-1}$ for liquid water at 0 °C, or $2{\cdot}834$–$2{\cdot}839 \times 10^6$ J $kg^{-1}$ for ice between 0 and −30 °C.

The model treats the soil as a moist, single layer system, with thickness equal to the depth of the temperature measurement, $z_g$ (m), and a temperature profile defined by input $T_g$ (K) at depth $z_g$, and the temperature of the lower snow layer, $T_{s,l}$, and therefore a vapour gradient between the snow/soil interface and a depth $z_g$ defined by saturation vapour pressures at $T_g$ and $T_{s,l}$. A base thermal conductivity for soil in mountainous regions, $K_g$ ($Jm^{-1}$ $K^{-1}$ $s^{-1}$), is set as a constant based on soil characteristics, using methods developed by Davis (1980). Base thermal conductivities for snow layers are set as functions of layer densities (Yen, 1965). A base diffusion coefficient $D_0$ ($m^2$ $s^{-1}$), is estimated for water vapour in snow or a saturated inorganic soil layer with a temperature of 0 °C at sea level pressure (Yen, 1965). Anderson (1976) developed an empirical relationship that can be used to adjust this base diffusion coefficient, $D_e$ (kg $m^{-1}$ $s^{-1}$ $K^{-1}$). $D_e$ is then used with base thermal conductivity and layer-specific humidity for the snow or soil to

 

compute an effective thermal conductivity that accounts for both heat conduction and vapour diffusion between layers

$$K_{es,0} = K_{s,0} + [L_v D_{e,0} q_{s,0}] \tag{7}$$

$$K_{es,l} = K_{s,l} + [L_v D_{e,l} q_{s,l}] \tag{8}$$

$$K_{eg} = K_g + [L_v D_{e,g} q_g] \tag{9}$$

$K_{es,0}$, $K_{es.l}$ and $K_{eg}$ ($Jm^{-1}\,K^{-1}\,s^{-1}$) are effective thermal conductivities for the surface and lower snow layers, and for the soil, $K_{s,0}$, $K_{s,l}$ and $K_g$ ($Jm^{-1}\,K^{-1}\,s^{-1}$) are base thermal conductivities for the surface and lower snow layers, and for the soil.

Energy transfer by conduction and diffusion between the soil and the lower layer of the snow cover, $G$ ($Wm^{-2}$), is calculated by

$$G = \frac{2K_{es,l}K_{eg}(T_g - T_{s,l})}{K_{eg}z_{s,l} + K_{es,l}z_g} \tag{10}$$

The depth of the soil measurement $z_g$ (m) is as an initial condition, and the soil temperature at $z_g$, $T_g$ (K), is an input data parameter. The temperature of the lower snow layer, $T_{s,l}$ (K), and the thickness of the lower snow layer, $z_{s,l}$ (m), are calculated by the model at each time-step.

Energy transfer by conduction and diffusion between the snow surface layer and the lower snow layer $G_0$ ($Wm^{-2}$) is calculated in the same manner

$$G_0 = \frac{2K_{es,0}K_{es,l}(T_{s,l} - T_{s,0})}{K_{es,l}z_{s,0} + K_{es,0}z_{s,l}} \tag{11}$$

The temperature of the surface snow layer, $T_{s,0}$ (K), and the thickness of the surface snow layer, $z_{s,0}$ (m), are calculated by the model at each time-step.

Advected energy transfer to the surface layer, $M$ ($Wm^{-2}$), is calculated only during time-steps when precipitation input has occurred

$$M = \frac{C_{p-p}\rho_{pp}z_{pp}[T_{pp} - T_{s,0}]}{t_{step}} \tag{12}$$

Advection is converted from a total ($Jm^{-2}$) to an average flux ($Wm^{-2}$) for the time-step by dividing by the length of the time-step in seconds, $t_{step}$. The density, mass, percentage snow and temperature of precipitation during the event are model inputs. From these, the model sets precipitation density, $\rho_{pp}$ (kg $m^{-3}$), precipitation depth, $z_{pp}$ (m), and precipitation temperature, $T_{pp}$ (K), as described below. The specific heat of precipitation, $C_{p-p}$, is calculated as a function of precipitation temperature, $T_{pp}$, and state (liquid or solid). If a mixed rain/snow event occurs, $C_{p-p}$ is estimated proportionally.

The surface energy exchange terms are summed to determine the net energy transfer to the surface snow layer $\Delta Q_0$ ($Wm^{-2}$)

$$\Delta Q_0 = R_n + H + L_v E + G_0 + M \tag{13}$$

and the total energy transfer to the snow cover

$$\Delta Q = \Delta Q_0 + G \tag{14}$$

 

These are used to determine the energy available for melting or refreezing in each layer. The energy available for melt or refreezing in each of the snow layers is (J $m^{-2}$)

$$Q_0 = \Delta Q_0 \times t_{\text{step}} + cc_{\text{s,0}} \tag{15}$$

$$Q_1 = (G - G_0) \times t_{\text{step}} + cc_{\text{s,l}} \tag{16}$$

$t_{\text{step}}$ is the time-step in seconds, and $cc_{\text{s,0}}$ and $cc_{\text{s,l}}$ (J $m^{-2}$) are the layer cold contents, or the energy required to bring the layer to $T_{\text{melt}}$. If $Q_0$ or $Q_1$ are positive, layer temperatures are set to $T_{\text{melt}}$, melt is calculated, the liquid water content of the snow cover is adjusted and the layer cold contents are set to 0. If $Q_0$ or $Q_1$ are negative, and liquid water is present, the energy required for refreezing is calculated, the liquid water content is adjusted, or set to 0, a new cold content is determined and the temperatures are adjusted for each layer.

If melt occurs during a time-step the thickness of the snow cover and snow cover layers, snow density, liquid water content and relative saturation are adjusted.

Evaporation or condensation between the snow surface layer and the atmosphere, $E$, was determined during the calculation of latent heat flux, $L_v E$. Evaporation or condensation between the lower snow layer and the soil $E_1$ (kg $m^{-2}$ $s^{-1}$) is calculated by

$$E_1 = \rho D_{\text{e,g}} \left[ \frac{q_{\text{g}} - q_{\text{s,l}}}{z_{\text{g}}} \right] \tag{17}$$

and the mass of evaporative loss or gain, $E_s$ (kg $m^{-2}$), is

$$E_s = (E + E_t) \times t_{\text{step}} \tag{18}$$

The specific mass of the snow cover is adjusted by the total mass of evaporative loss or gain. If liquid water is present, it is preferentially evaporated by the ratio of the latent heat of vaporization to sublimation at 0 °C (0·882). The snow cover liquid water content is then adjusted for evaporation. The remaining evaporative loss, or all evaporation after liquid water has been depleted, is modelled as sublimated ice. Half of the ice lost is assumed to be decreased depth. The remaining sublimated ice and all evaporated liquid water decrease the density and mass of the snow cover, so again snow cover thicknesses, density and liquid water capacity are adjusted. If the total liquid water exceeds the adjusted liquid water capacity, the excess becomes runoff, and snow density and specific mass are adjusted.

## CLIMATE DATA

From Figure 2 we can see that the two-month period from 1 January to 28 February 1996 can be broken into segments based on climatic conditions. 1–11 January was prior to the development of a significant snow cover at either the mid- or high sites; 12–27 January was when extensive snow cover was deposited; and 27 January–2 February was a very cold, fairly clear period. The main thrust of the rain-on-snow even occurred from 3–8 February, followed by a warm, clear period from 9–16 February, and then a cooler storm that started as rain and then turned to snow from 16–22 February. After 22 February climate conditions returned to cooler winter conditions.

Table I lists the parameters monitored at the mid- and high sites. Of these, solar radiation, air and soil temperature at (30 cm), humidity, wind speed and precipitation were used to drive the simulation of snow processes and properties. Figure 4 shows hourly averages for net solar radiation, wind speed, vapour pressure, air and soil temperature at the open and forested high sites and at the open mid-site during the period from 1 January to 28 February 1996.

During the entire two months little difference is shown between air temperature or vapour pressure at the three sites. It appears to be about 1 °C warmer, and slightly more humid at the mid-site, which is what would be expected for a 200 m elevation difference. Soil temperature is also similar at all three sites when a snow

 

cover is present. The higher soil temperatures, with indication of a diurnal cycle, occur at the mid-site when the snow cover is not present and solar heating of the soil is possible. Once the snow cover is established, soil temperatures are nearly identical at all three sites. Net solar radiation in the open at both the mid- and high sites is nearly identical. As expected, net solar radiation at the forested high site is only about 25% of that in the open, most of the time. Thermal radiation was not measured, but was calculated from air temperature, humidity, air pressure and canopy cover using a method developed by Marks and Dozier (1979). Wind speeds in the open at the mid- and high sites are similar, with winds being slightly less during some periods at the mid-site. Wind speeds at the forested high site are generally only about 15–25% of wind speeds in the open, nearly all the time.

Air temperatures, vapour pressure and solar radiation clearly show the period of development of the snow cover (12–27 January), followed by the very cold period that followed (28 January to 2 February). In contrast, climate conditions during the rain-on-snow event show a reduction in solar radiation, air temperatures always above freezing and an increase in vapour pressure to well above the saturation vapour pressure at 0 °C. Air and soil temperatures, vapour pressure and radiation in the open at the mid- and high sites are similar during the event. However, under the forest canopy at the high site it was cooler, less humid and solar radiation was reduced.

Figure 5 shows means solar radiation, wind speed, vapour pressure and air temperature for the three sites during each of the climate periods. Air temperature is shown as the departure from 0 °C (611 Pa). Wind speed is shown on an exponential scale, to illustrate the effect a modest increase in long-term average wind speed will have on turbulent fluxes [see Equations (3)–(6)]. During the rain-on-snow event, air temperatures were above freezing, and there was a large humidity gradient towards the snow cover at all three sites. Although there were small differences in solar radiation between the forested and open sites, and most significant climatic difference between the forested and open sites during the rain-on-snow event was that wind speeds were high at both open sites, but not at the forested site.

## SNOW COVER ENERGY AND MASS BALANCE SIMULATION

### *Snow cover energy balance*

The snow cover energy balance model was run at an hourly time-step from 1 January to 28 February 1996, using data from the open clear-cuts at the mid- and high sites, and for the forested location at the high site. Figure 6 presents the hourly average of the sum of the energy balance terms $\Delta Q$, net all-wave radiation $R_n$ soil heat flux $G$, advected heat flux $M$ and the latent $L_vE$ and sensible heat flux $H$ for these three sites. Figure 7 presents the relative energy fluxes for $R_n$, $G$, $M$ and the sum of the turbulent fluxes, $H + L_vE$, for the high open and forested, and mid- open sites. In Figure 7, the size of the overall coloured bar is based on the average of $\Delta Q$ during the climatic period. The relative importance of each of the energy flux parameters, $R_n$, $G$, $M$, and the 'net turbulent flux' ($L_vE + H$) are shown as coloured portions of the bar.

On 1 January, all three sites were snow free. The model developed a snow cover as precipitation events occurred. The model produces output only when snow is present, so during much of the first half of January all output parameters are set to zero. A few minor deposition events occurred during the first week in January, but these melted rapidly and did not persist for more than a day or so.

Development of the snow cover at the sites occurs during the period from 15–26 January. During this time, the snow cover energy balance is at or near zero, with a diurnal oscillation from day to night conditions. During the cold period from 27 January to 2 February the magnitude of the energy balance increases, with a more pronounced diurnal cycle in the open. Although it was cold during this period, snow cover energy flux was generally in balance (see Figures 6 and 7), and the cold content of the snow cover did not increase substantially. During this time $L_vE$ and $H$ display a common characteristic which occurs during non-storm periods (see Marks and Dozier, 1992). they are of the same magnitude, but opposite in sign, so the 'net turbulent flux' ($L_vE + H$) is close to zero. $G$ and $M$ are effectively zero also, so $R_n$ is the dominant energy balance term during this period. The diurnal character of the energy balance is much more

 

pronounced at the open sites. The snow cover energy balance at the forested site shows the same characteristics, but is very damped, and near zero.

During the ROS event the snow cover energy balance is quite different as all three sites have a distinctly positive energy balance, with a large input of energy at the open sites. $R_n$ is damped, without a strong diurnal character, and though slightly negative contributes only about 15–20% of $\Delta Q$ in the open, and about 30% under the forest. $G$ is still small, but $M$, advected heat from rain, begins to make a contribution only slightly smaller than $R_n$ to the snow cover energy balance at all three sites.

The most important difference, however, is in $H$ and $L_vE$. During the ROS event, both were positive, and combined to enhance the snow cover energy balance significantly. This condition occurs beneath the forest, where $L_vE + H$ represented about 35% of $\Delta Q$, but was most pronounced at the open sites, where $L_vE + H$ represented 75–80% of $\Delta Q$. The result is that $\Delta Q$ is large and positive throughout the ROS event, providing a substantial amount of energy for snowmelt.

During the period immediately following the ROS event (9–15 February), the energy balance was still positive, though somewhat smaller in magnitude than during the ROS event. Air temperatures were still warm, humidities well above saturation at 0 °C and, under clear skies, $R_n$ becomes a more significant component of $\Delta Q$, representing 60–75% of total energy at all three sites. The diurnal cycle returns, and though $L_vE$ and $H$ begin to again have opposite magnitudes, $L_vE + H$ is still positive, but now represents only 15–25% of $\Delta Q$. $M$ was not a factor once precipitation stopped. Because of the influence of large volumes of 0 °C melt-water percolating into the soil column, the temperature gradient between the soil and the snow [see Equation (11)] is removed, and $G$ is unimportant at both the open and forested high sites. However, at the mid-site, $G$ begins to increase as the snow cover thins and the soil begins to be heated by solar radiation during the day, contributing nearly 25% of the energy in $\Delta Q$ at the open mid-site. $R_n$ is once again the dominant term in the snow cover energy balance, providing energy for melt during the day, and then cooling the snow cover at night.

During the rain/snow event (17–21 February), and the clear post-storm period that followed (22–28 February) the snow cover energy balance was similar to conditions during, and immediately following the development of the snow cover (12 January–2 February). In general, $\Delta Q$ is small at all three sites. $R_n$ is damped, without a strong diurnal character during the storm, and then close to zero following the storm. $H$ and $L_vE$ are damped and near zero, and both $M$ and $G$ are unimportant because the temperature gradients are small [see Equations (11) and (12)]. ($G$ is somewhat larger at the mid-site because the snow cover is thin and solar radiation is penetrating to heat the soil.)

*Snow cover mass balance*

In addition to snow cover energy balance terms, the model predicts evaporation from, or condensation on, the snow cover, snowmelt and runoff from the base of the snow cover. Figure 8 presents evaporation or condensation, snowmelt and runoff at both the open and forested sites during the run. Evaporation from the snow cover is shown as a negative mass flux, while condensation on the snow cover is shown as a positive mass flux. Generally, these terms are small, with a diurnal character that oscillates between day and night. The one exception to this pattern is during the ROS event, when significant condensation occurred during both day and night at the open sites. Evaporation or condensation is always small at the forested sites.

The model converts rain directly to runoff even when no snow is present. When snow is present, runoff is the sum of melt, less the liquid $H_2O$ holding capacity of the snow cover, plus rain. At all three sites, most of the January runoff was direct rainfall. During the ROS event melt and runoff have very little diurnal character. Just over half the runoff in the open at the high site was from snowmelt, while in the open at the mid-site, just less than half was from snowmelt. Most of the runoff from the high site forest was from rain.

During the clear period following the ROS event, runoff was derived from melt, and both melt and runoff had a strong diurnal character. More melt occurred in the open at the mid-site, than at the high site, until the snow cover was depleted late on 14 February at the mid-site. While melt occurred at the forested site, it amounted to only about 15–20% of the runoff from the mid-site, which was substantially less than at either open site.

 

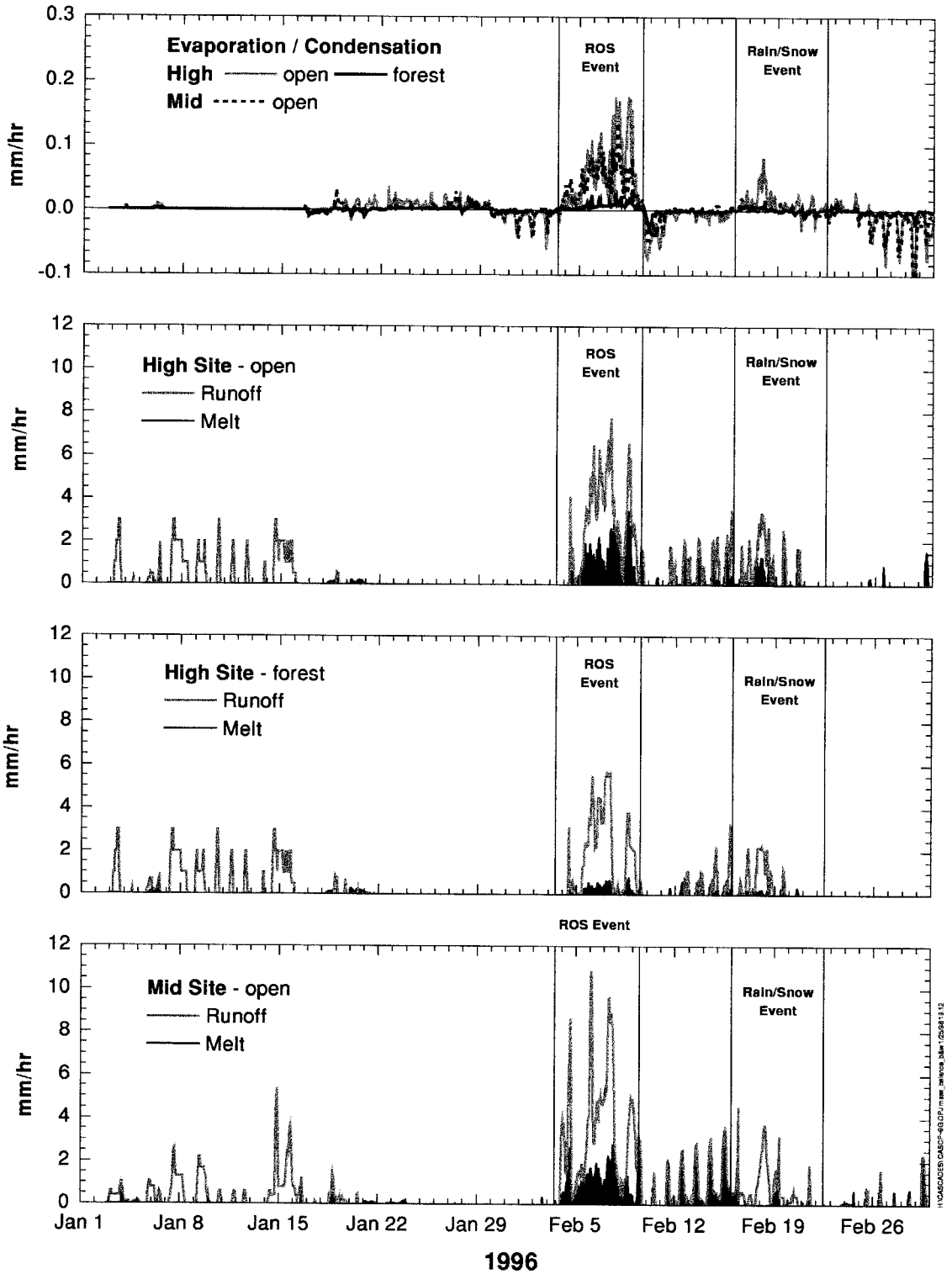


Figure 8. Hourly mass fluxes from or to the snow cover from evaporation, condensation, snowmelt and runoff for each of the experimental sites

 

At the beginning of the rain/snow event, runoff occurred from rain and a small amount of melt at all three sites. After 19 February, no melt or runoff occurred at the forested site, and only a small amount of melt occurred in the open at the high site. More melt occurred at the open mid-site than in the open high site because the snow cover is thin, and temperatures are warmer.

*Model verification*

Data on snow depths in the open at the mid- and high sites, along with data from two nearby SNOTEL stations are used to verify the simulated snow cover energy and mass characteristics. SNOTEL stations are generally 'open' sites, but some are more protected than others. The two selected for this analysis are located in distinctly open locations. The Daly Lake SNOTEL station was selected as most representative of conditions at the high site clear-cut. It is nearby, and occupies a similar elevation (1100 m vs. 1142 m for the high site) and is in an open site near the western Cascade crest. The Marion Forks SNOTEL station was selected as most representative of conditions at the mid-site clear-cut. It is nearby, and occupies an exposure with a similar fetch. It is 129 m lower, but the SWE and precipitation inputs during the 60-day period of the simulation are similar. Neither the SNOTEL nor snow depth data were used to initialize, calibrate or drive the simulations.

Figure 9 presents a comparison between modelled snow cover mass and depth during the simulation period. Simulated SWE in the clear-cut at the high site is similar to SWE from the Daly Lake SNOTEL station. The maximum SWE at Daly Lake is slightly larger (5–8%) than the simulated value in the high site just prior to the ROS event. The SWE depletion curves during and just after the ROS event, and redevelopment of the snow cover after 17 February are nearly identical in shape. Simulated snow depth in the clear-cut at the high site closely matches measured values, both during the development of the snow cover, and during the ROS event. Neither depth nor SWE data were available for the forested site. The simulated values for SWE and snow depth at the forested site are presented for comparison with the snow cover in the open. The symbols shown in Figure 9 represent point measurements of snow depth taken on 17 February, during a visit to the high site following the ROS event. These measurements indicate that the relative differences between simulated snow depth in the open and forested sites are reasonable.

Simulated SWE in the clear-cut at the mid-site matches SWE from the Marion Forks very closely during development of the snow cover prior to the ROS event, and during snow deposition during the latter part of February. The simulated depletion of SWE from the snow cover is, however, much more gradual than data from the SNOTEL station would indicate. Comparison of the simulated snow depth to measured snow depth at the mid-site indicates that snow at that site was depleted during the ROS event in a manner matched by the simulation.

Both Marion Forks and Daly Lake show a spike of increased SWE just prior to the onset of melt. This spike could have occurred because the storm started out as snow and then became rain. However, maximum and minimum air temperature data from these SNOTEL stations, and climate data from the central Cascade experimental sites, suggest that no snow fell at the experimental sites during the event. Both air and dew point temperatures were well above freezing just prior to and throughout the event. A more likely explanation is evident in the Marion Forks SWE trace (see Figures 2 and 9). It shows a rapid increase in SWE as the ROS event began that is suddenly halted on 5 February, and then in a few hours nearly all the SWE over the snow pillow is lost. From Figure 4 we see that soil temperatures were above freezing prior to the ROS event, dropping to near 0·0 °C as liquid water began to percolate into the soil soon after it started. Because the snow pillow alters the thermal and moisture exchange between the soil and snow, and because the soil was quite moist, we can assume that a significant transfer of vapour from the soil to the cold snowpack, with its associated heat, would have taken place prior to the ROS event. This vapour transfer could not have occurred over the snow pillow, so we also assume that the snow over the snow pillow would be colder and may have contained basal ice. Rain water was probably retained above the snow pillow until the thermal gradient was removed, and the ice layers melted. At that time a sudden reduction in SWE occurred, much like the breaking of an ice dam, which would explain the sudden catastrophic loss of SWE reported by the Marion Forks SNOTEL station during the ROS event. This assessment offers a possible explanation for the spikes that show

 

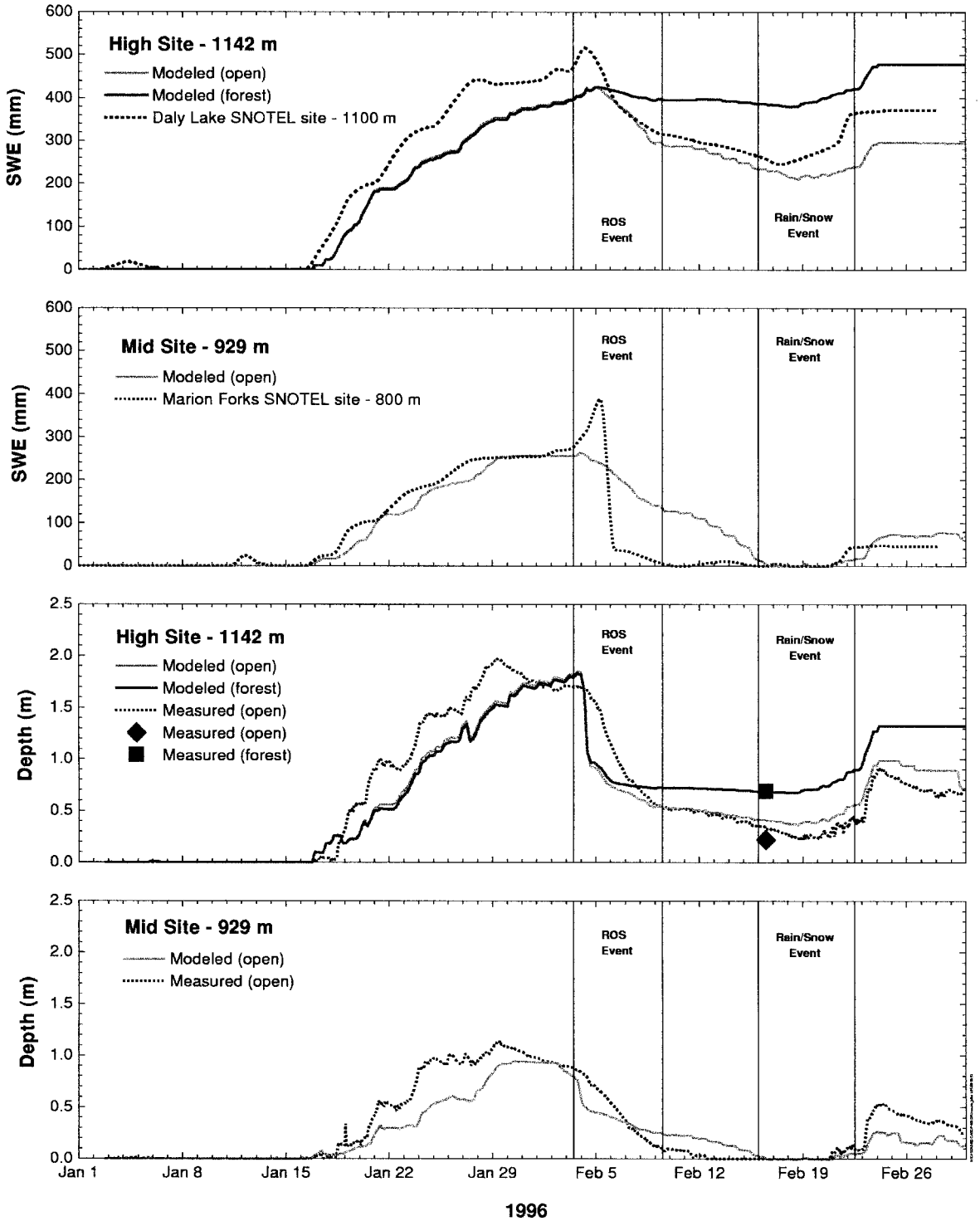


Figure 9. Comparison of measured and modelled snow cover depth and snow water equivalent (SWE) for each of the experimental sites for the period 1 January to 1 March 1996. Point measurements of snow depth at the high site in the open and the forest, taken during a site visit on 17 February 1996, are also indicated

 

in the SWE traces, shown in Figure 2, for Hogg Pass, Little Meadows and Daly Lake as well. Ultimately, this assessment must be considered speculation, because observations of snow pillow response during an event of this magnitude are non-existent, and no data exist on differences between snow thermal and moisture characteristics over snow pillows and over the soil surface during rain-on-snow.

## CONCLUSIONS

The energy balance snowmelt model used in this study accurately simulated snow cover mass (SWE) and depth during the development and ablation of the snow cover prior to, during and following one of the most extreme rain-on-snow events on record. The relative magnitude of the energy balance terms, particularly the importance of the turbulent transfer terms $H$ and $L_vE$ during rain-on-snow shows how the combination of warm air temperatures, high winds and high humidities can cause significant condensation on the snow surface, providing adequate energy for rapid melting of the snow cover. Both SNOTEL SWE data and experimental site snow depth data verify that rapid depletion of the snow cover did occur. Snowmelt was a significant component of the runoff which caused the February 1996 flood from the Oregon Cascade Mountains. Model results indicate that melt that occurred during this flood was caused by condensation on the snow surface during the event. These conditions were enhanced by high winds, warm air temperatures and high humidities during the event, and by the fact that a cold storm had deposited significant snow cover down to relatively low elevations within the snow transition zone.

Although precipitation, air temperature, humidity and radiation were similar at the forested and open sites, wind speeds were significantly lower at the forested site. The model showed only 48 mm of melt under the forest during the event, but 235 mm of melt in the clear-cut at the high site, and 258 mm of melt in the clear-cut at the mid-site.

In the snow transition zone of the central and northern Cascade Mountains forest clear-cutting is common. Forest cover reduces wind speed, which reduces the turbulent fluxes, and therefore reduces the generation of snowmelt during rain-on-snow. This analysis shows that during this event, the generation of snowmelt was enhanced in forest openings and clear-cuts.

This analysis also illustrates the importance of the interaction between forest canopies and hydrological processes. It also shows the value of climatic monitoring in both open and forested sites within the snow transition zone. Although an event of this magnitude does not occur frequently, several similar events have occurred in the past 2–3 years, causing devastating floods in Reno, Nevada; Boise, Idaho; Seattle, Washington; and Portland, Oregon.

Conditions during the February 1996 flood were extreme and were enhanced by the antecedent conditions, which deposited significant amounts of snow down to relatively low elevations. Runoff and flooding were enhanced by snowmelt caused by condensation on the snow cover during the event. The results of this analysis show differences in how snowmelt is generated at open and forested sites during rain-on-snow conditions. Even if all sites had been forested, significant runoff would have occurred, but substantially more snowmelt and runoff was generated in the open, clear-cuts than under the forest canopy. The model presented in this paper could be used to assess the potential for snowmelt generation and flooding under different forest management schemes.

### ACKNOWLEDGEMENTS

We gratefully acknowledge the assistance of Robert McKane for processing and checking meteorological data from the field sites, and Glenn Jarrell for site maintenance during the period of this study. The information in this document has been funded by the US Environmental Protection Agency under Interagency Agreement DW14936911 with the US Geological Survey. It has been subject to EPA and USGS review, and approved for publication. Mention of trade names or commercial products does not constitute endorsement or recommendation for use.

 

## REFERENCES


Anderson, E. A. 1976. 'A point energy and mass balance model of a snow cover', *NWS Technical Report 19*. National Oceanic and Atmospheric Administration, Washington, DC. 150 pp.

Beaudry, P. and Golding, D. L. 1983. 'Snowmelt during rain-on-snow in coastal British Columbia', *Proceedings of the Western Snow Conference*, **51**, 55–66.

Berris, S. and Harr, R. D. 1987. 'Comparative snow accumulation and melt during rainfall in forested and clear-cut plots in the western Cascades of Oregon', *Wat. Resour. Res.*, **23**, 135–142.

Brutsaert, W. 1982. *Evaporation into the Atmosphere*. D. Reidel, Dordrecht, 299 pp.

Coffin, B. and Harr, R. D. 1992. 'Effects of forest cover on volume of water delivery to soil during rain-on-snow'. *Timber/Fish/Wildlife Report SH1-92-001*. Washington Department of Natural Resources, Olympia, Washington. 118 pp.

Colbeck, S. C. 1978. 'The difficulties of measuring the water saturation and porosity of snow', *J. Glaciol.*, **20**, 189–201.

Colbeck, S. C. 1982. 'An overview of seasonal snow metamorphism', *Rev. Geophys. Space Phys.*, **20**, 45–61.

Colbeck, S. C., Anderson, E. A., Bissel, V. C., Crook, A. G., Male, D. H., Slaughter, C. W. and Wiesnet, D. R. 1979. 'Snow accumulation, distribution, melt, and runoff", *EOS, Trans. Am. Geophys. Union*, **60**, 465–474.

Davis, R. E. 1980. 'Simulation of an alpine soil thermal regime beneath a snowpack', *MA Thesis*, Department of Geography, University of California, Santa Barbara, 60 pp.

Davis, R. E., Dozier, J. and Marks, D. 1984. 'Micrometeorological measurements and instrumentation in support of remote sensing observations of an alpine snow cover', *Proceedings of the Western Snow Conference*, **52**, 161–164.

Davis, R. E., Dozier, J., LaChapelle, E. R. and Perla, R. 1985. 'Field and laboratory measurements of snow liquid water by dilution', *Wat. Resour. Res.*, **21**, 1415–1420.

Harr, R. D. 1986. 'Effects of clearcutting on rain-on-snow runoff in western Oregon: a new look at old studies', *Wat. Resourc. Res.*, **22**, 1095–1100.

Jones, J. A. and Grant, G. E. 1996. 'Peak flow responses to clear-cutting and roads in small and large basins, western Cascades, Oregon', *Wat. Resourc. Res.*, **32**, 959–974.

Jordan, R. 1991. 'A one-dimensional temperature model for a snow cover: technical documentation for SNTHERM.89', Special Report 91-16, US Army Corps of Engineers Cold Regions Research and Engineering Laboratory, Hanover, 49 pp.

Kattelmann, R. 1989. 'Spatial variability of snowpack outflow at a Sierra nevada site', *Ann. Glaciol.*, **13**, 124–128.

Male, D. H. and Granger, R. J. 1981. 'Snow surface energy exchange', *Wat. Resour. Res.*, **17**, 609–627.

Marks, D. 1988. 'Climate, energy exchange, and snowmelt in Emerald Lake watershed, Sierra Nevada', *PhD Thesis*, Departments of Geography and Mechanical Engineering, University of California, Santa Barbara. 158 pp.

Marks, D. and Dozier, J. 1979. 'A clear-sky longwave radiation model for remote alpine areas', *Arch. Meteorol. Geophys. Bioklimatol. Ser. B*, **27**, 159–187.

Marks, D. and Dozier, J. 1992. 'Climate and energy exchange at the snow surface in the alpine region of the Sierra Nevada: 2. Snow cover energy balance', *Wat. Resour. Res.*, **28**, 3043–3054.

Marks, D., Kattelmann, R., Dozier, J. and Davis, R. E. 1986. 'Monitoring snowcover properties and processes in a small alpine watershed', in *Proceedings of Sixth International Northern Research Basins Symposium/Workshop*. Santeford, H. S. (ed.), Michigan Technological University, Houghton, pp. 259–275.

Marks, D., Dozier, J. and Davis, R. E. 1992. 'Climate and energy exchange at the snow surface in the alpine region of the Sierra nevada: 1. Meteorological measurements and monitoring', *Wat. Resour. Res.*, **28**, 3029–3042.

Marks, D., Domingo, J. and Frew, J. 1998. 'Software tools for hydro-climatic modeling and analysis: Image Processing Workbench, ARS-USGS Version 2.0'. Electronic Document http://quercus.ars.pn.usbr.gov/~ipw. Northwest Watershed Research Center, USDA Agricultural Research Service, Boise, Idaho.

Morris, E. M. 1982. 'Sensitivity of the European Hydrological System snow models', in Glen, J. W. (ed.), *Hydrological Aspects of Alpine and High-Mountain Areas*, IAHS–AIHS Publication 138. International Association of Hydrological Sciences, Wallingford. pp. 221–231.

Morris, E. M. 1986. 'Modelling of a seasonal snowcover', in Kukla, G., Barry, R. G., Hecht, A. and Wiesnet, D. (eds), *Snow Watch '85*. Glaciological Data report GD-18. World Data Center for Glaciology, Boulder. pp. 225–240.

Smith, J. L. and Berg, N. 1982. *The Sierra Ecology Project*, Vol. III. Pacific Southwest Forest and Range Experiment Station, USDA Forest Service, Berkeley, California. 104 pp.

Tarboton, D. G., Chowdhury, T. G. and Jackson, T. H. 1995. 'A spatially distributed energy balance snowmelt model', in Tonneson, K. A., Williams, M. and Tranter, M. (eds), *Biogeochemistry of Seasonally Snow Covered Catchments*, IAHS–AIHS Publication 228. International Association of Hydrological Sciences, Wallingford. pp. 141–155.

USDA Soil Conservation Service 1988. *Snow Survey and Water Supply Products Reference*. USDA-SCS Western National Technical Center, Portland, OR.

van Heeswijk, M., Kimball, J. and Marks, D. 1996. 'Simulation of water available for runoff in clearcut forest openings during rain-on-snow events in the western Cascade Range of Oregon and Washington', *Water-Resources Investigations Report 95-4219*. US Geological Survey, Tacoma, Washington,. 67 pp.

Waananen, A., Harris, D. and Williams, R. 1971. 'Floods of December 1964 and January 1965 in the Far Western States, Part 1. Description', *Water Supply Paper 1866-A*. US Geological Survey, Washington, DC. 265 pp.

Yen, Y.-C. 1965. 'Heat transfer characteristics of naturally compacted snow', *Technical Report 166*. US Army Cold Regions Research and Engineering Laboratory, Hanover. 9 pp.


 

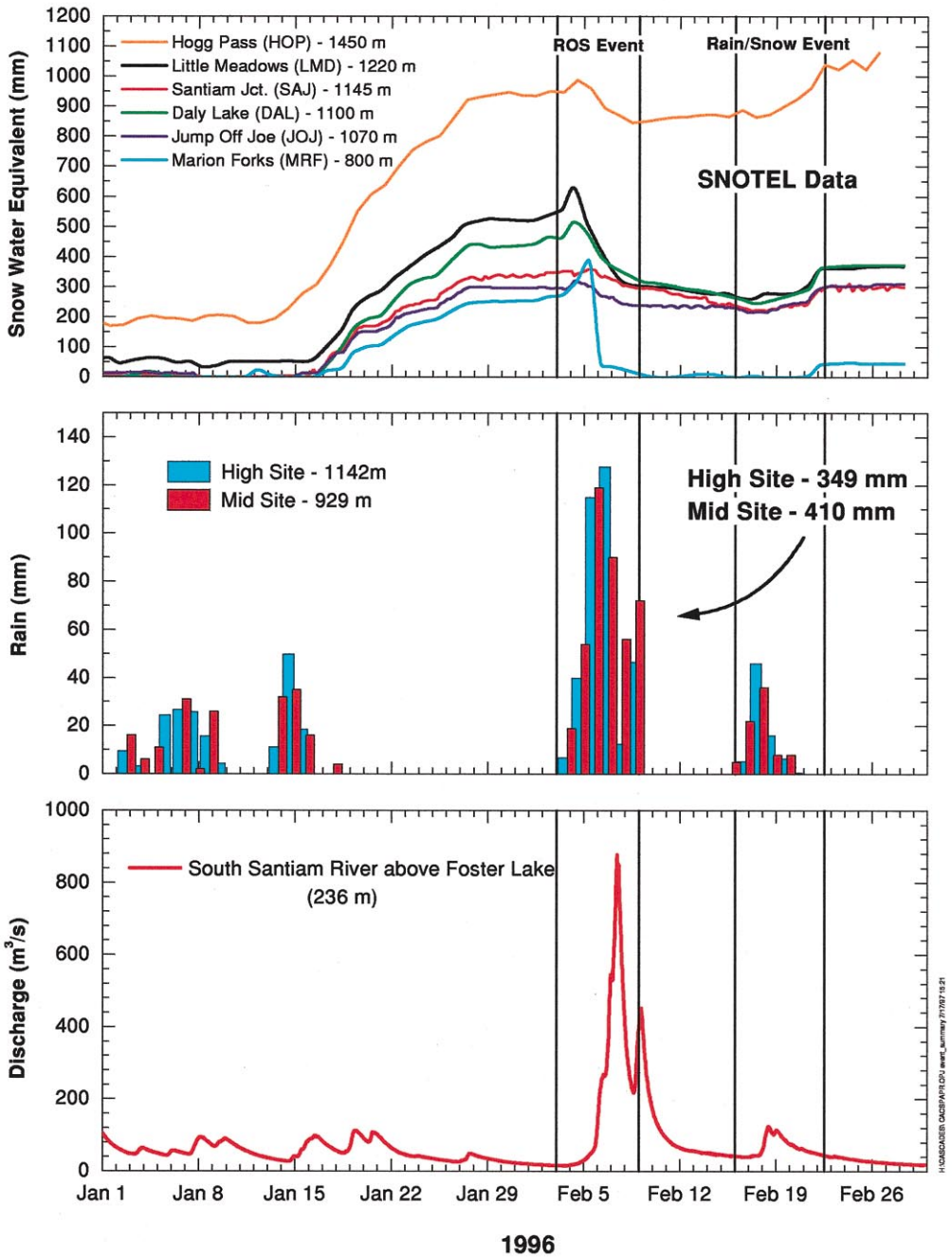


Figure 2. Hourly traces from the six nearest NRCS SNOTEL stations, daily rainfall recorded at the mid- and high experimental sites and half-hourly stream discharge measured just above Foster Lake, on the South Santiam River, from 1 January to 1 March, 1996. Only rain was recorded at the high and mid-sites, because the unheated tipping bucket gauges used do not collect snowfall

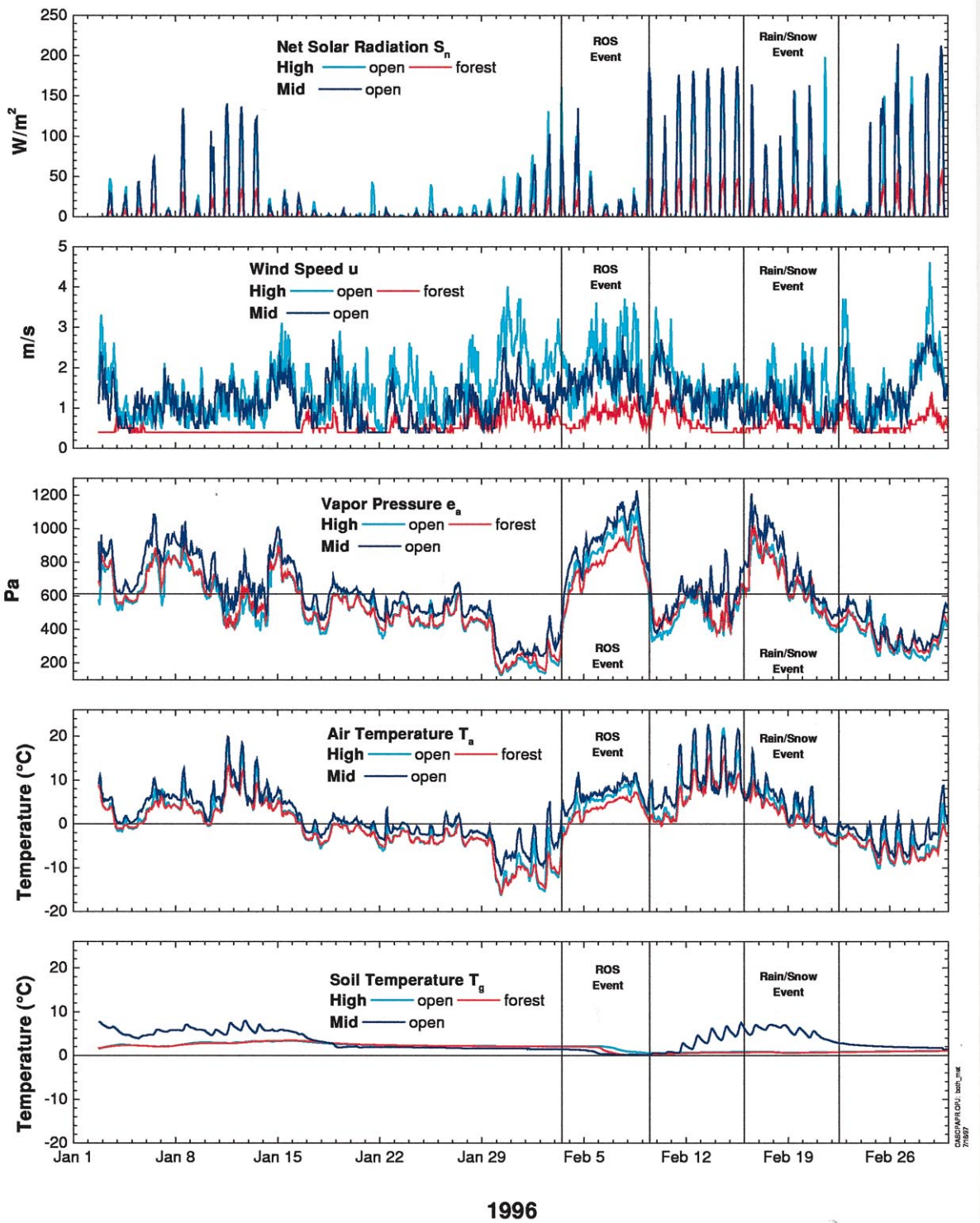


Figure 4. Hourly net solar radiation ($S_n$), wind speed ($u$), vapour pressure ($e_a$), air temperature ($T_a$) and soil temperature ($T_g$) at 30 cm, measured at the mid-site in the open, and the high site in both the open and under the forest for the period 1 January to 1 March, 1996

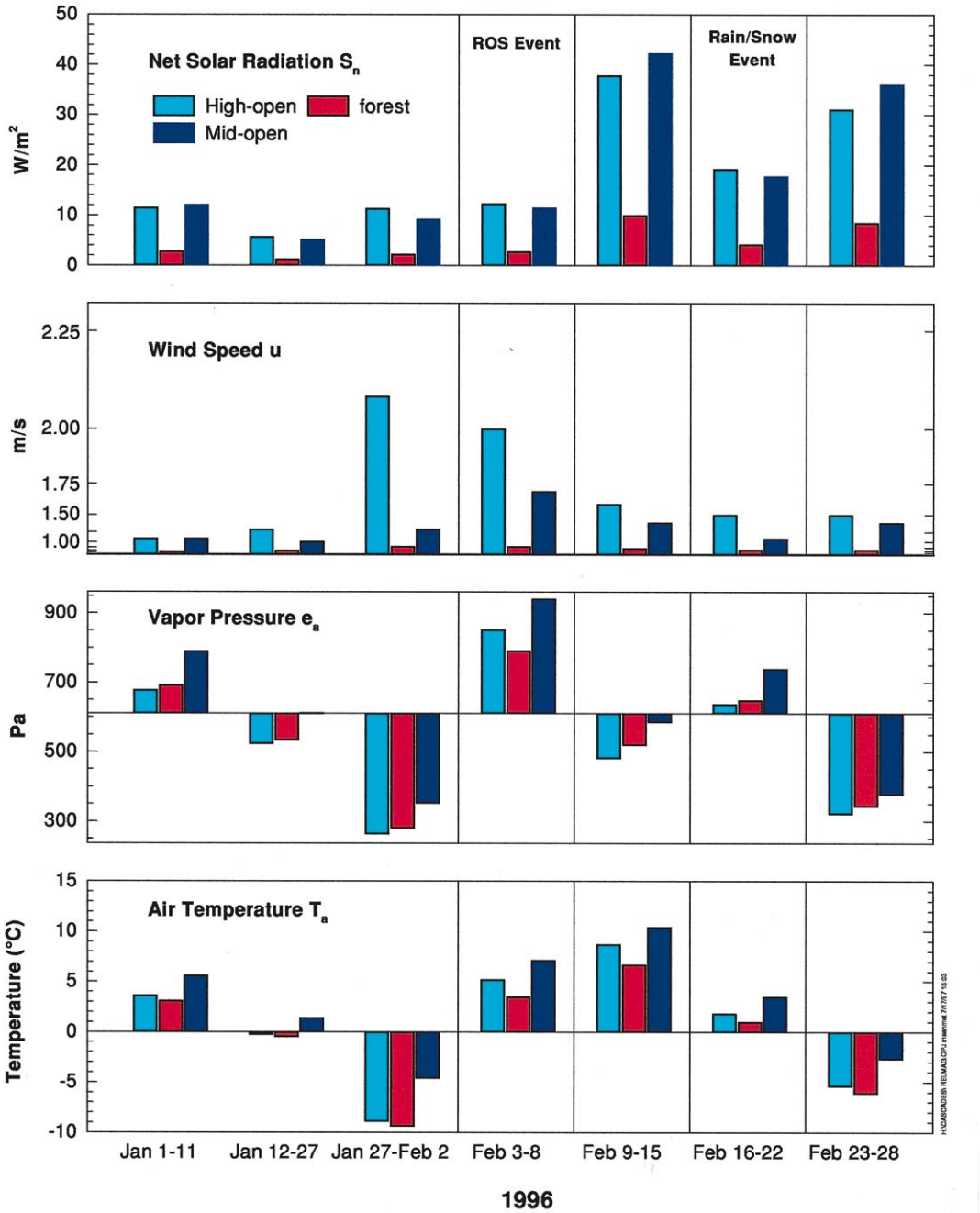


Figure 5. Mean net solar radiation ($S_n$), wind speed ($u$), vapour pressure ($e_a$) and air temperature ($T_a$) for the three sites during the seven climate periods

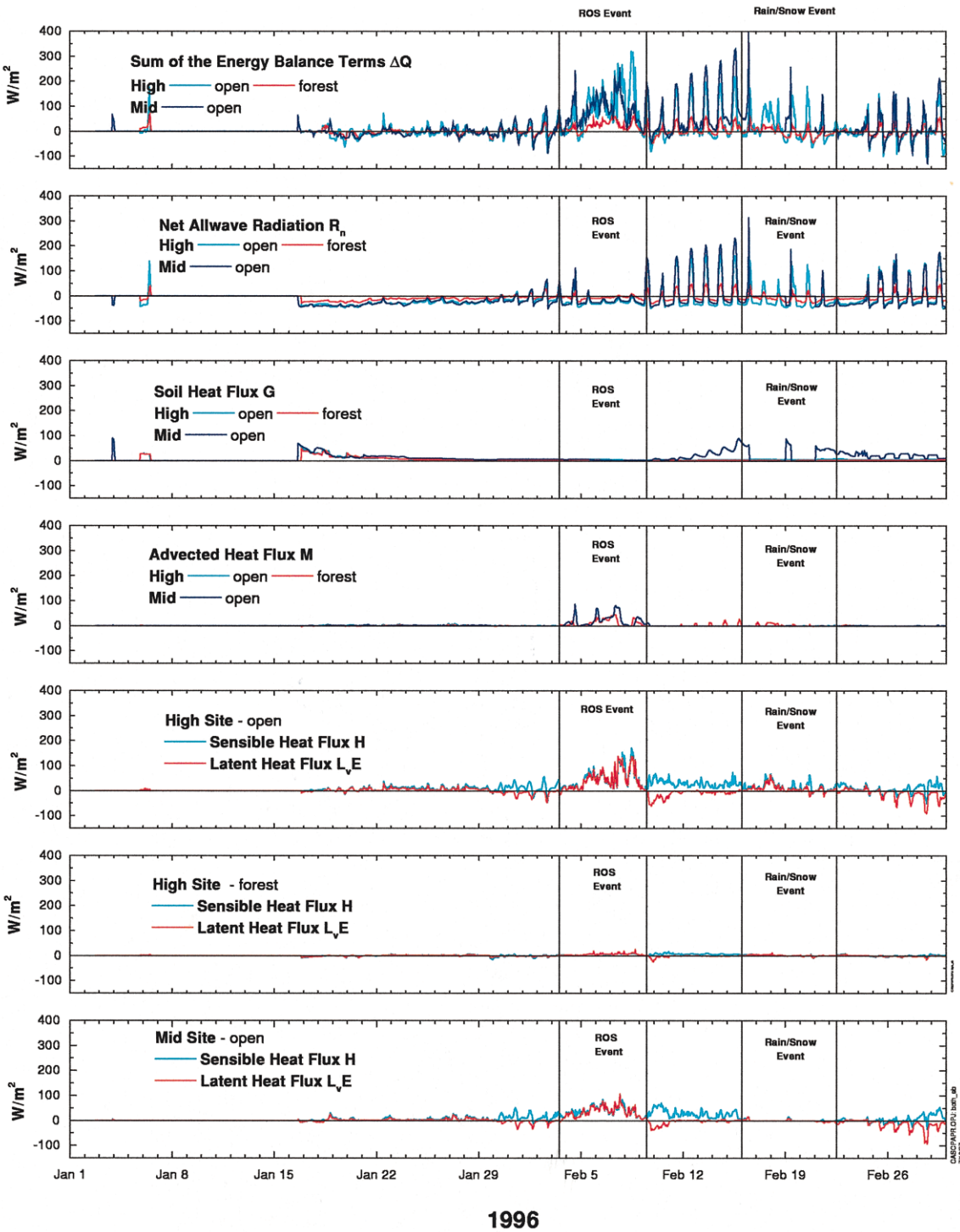


Figure 6. Hourly average snow cover sum of the energy balance terms ($\Delta Q$), net all-wave radiation ($R_n$), soil heat flux ($G$), advected heat flux ($M$) and sensible and latent heat fluxes ($H$ and $L_vE$) for each of the experimental sites for the period 1 January to 1 March 1996. Note that the energy balance is not calculated for periods in which no snow cover is present

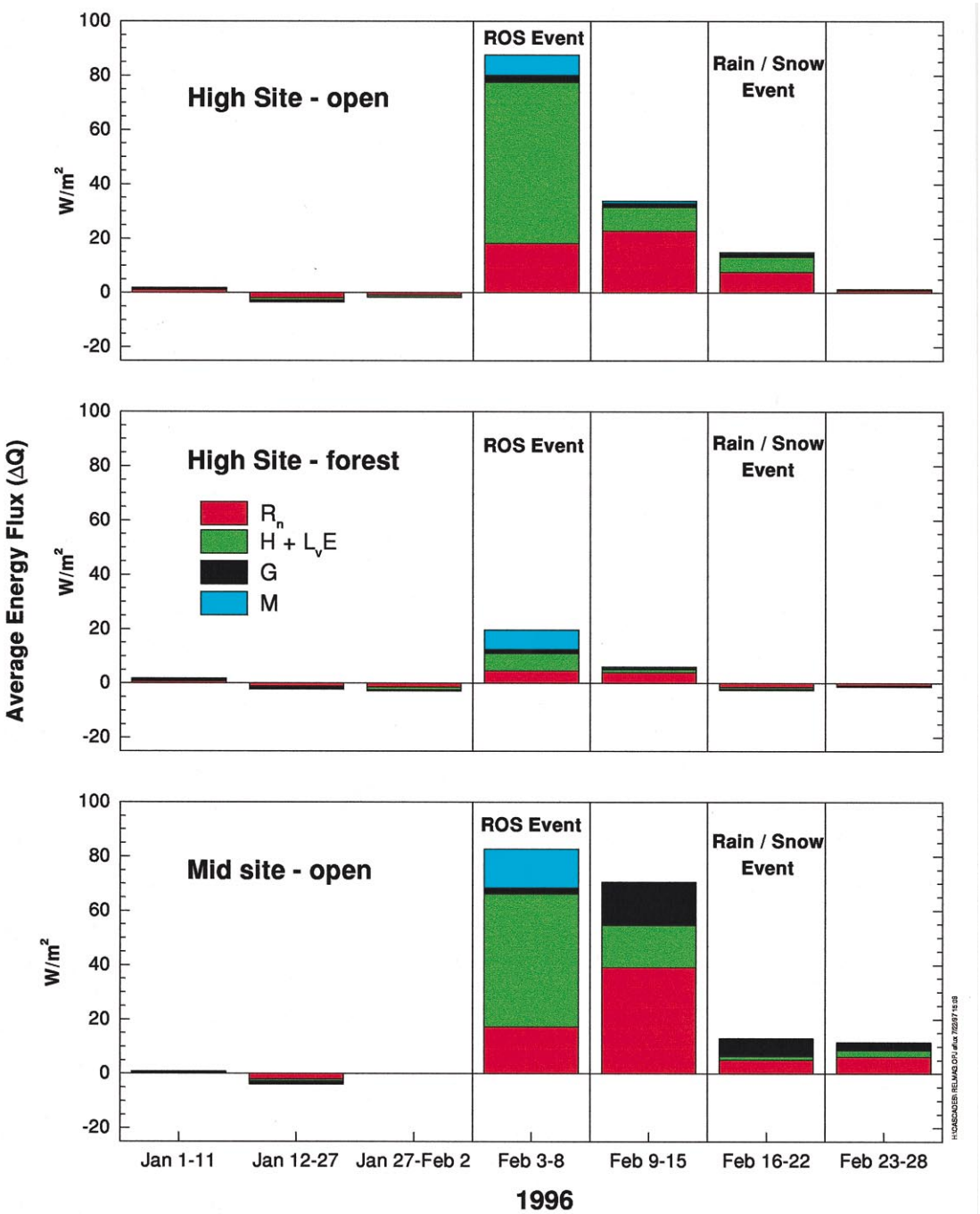


Figure 7. Average energy flux ($\Delta Q$) and the contributions from net all-wave radiation ($R_n$), soil heat flux ($G$), advected heat flux ($M$) and the sum of sensible and latent heat fluxes ($H + L_vE$), for each of the experimental sites during the seven climate periods. The size and sign of the coloured bar is based on the average magnitude and sign of the sum of the energy balance terms ($\Delta Q$) during each climate period, and the relative contribution of each energy flux term is represented as the portion of the bar made up by that colour